

Article

Effect of Cold Rolling on the Phase Transformation Kinetics of an $\text{Al}_{0.5}\text{CoCrFeNi}$ High-Entropy Alloy

Jun Wang , Haoxue Yang, Tong Guo, Jiayang Wang, William Yi Wang  and Jinshan Li

State Key Laboratory of Solidification Processing, Northwestern Polytechnical University, Xi'an 710072, China; hxyang@mail.nwpu.edu.cn (H.Y.); believegt@163.com (T.G.); 2013301034@mail.nwpu.edu.cn (J.W.); wywang@nwpu.edu.cn (W.Y.W.); ljsh@nwpu.edu.cn (J.L.)

* Correspondence: nwpuwj@nwpu.edu.cn; Tel.: +86-29-88460568; Fax: +86-29-88460294

Received: 25 October 2018; Accepted: 29 November 2018; Published: 30 November 2018



Abstract: The solid state phase transformation kinetics of as-cast and cold rolling deformed $\text{Al}_{0.5}\text{CoCrFeNi}$ high-entropy alloys have been investigated by the thermal expansion method. The phase transformed volume fractions are determined from the thermal expansion curve using the lever rule method, and the deformed sample exhibits a much higher transformation rate. Two kinetic parameters, activation energy (E) and kinetic exponent (n) are determined using Kissinger–Akahira–Sunose (KAS) and Johnson–Mehl–Avrami (JMA) method, respectively. Results show that a pre-deformed sample shows a much lower activation energy and higher kinetic exponent compared with the as-cast sample, which are interpreted based on the deformation induced defects that can promote the nucleation and growth process during phase transformation.

Keywords: high-entropy alloy; phase transformation; kinetics; deformation; thermal expansion

1. Introduction

High-entropy alloys (HEAs) are a new class of alloys designed based on a unique alloy concept that have multi alloy components (normally five or more principal elements) with equal or near-equal atomic composition [1,2]. HEAs are mainly solid solution based alloys, which own very attractive properties, like high strength and hardness, high fracture toughness, excellent corrosion resistance and unique physical properties, making them the potential engineering materials in many industry areas [3–7].

Thermal induced phase transformations are one of the main transitions inside metallic materials which can be used to control the final phases of the material, and thus to tune the properties. In order to know the details of the phase transformation processes, one of the useful methods is to study the phase transformation kinetics, which can give a lot of useful information like phase transformation speed and transition mode [8,9]. However, until now, there have only been very few papers referring to the kinetic analysis of high-entropy alloys.

The as-cast HEAs always exhibit coarse grains especially for big ingots. In order to obtain fine equiaxed grains, methods like cold rolling or forging are incorporated during the treating process [10,11]. Whether this kind of treatment can affect the subsequent phase transformation process is still unclear for HEAs.

$\text{Al}_x\text{CoCrFeNi}$ ($0 \leq x \leq 2$) HEAs are one of the alloy systems that intrigue the research interest due to many aspects. First, this alloy system owns very good mechanical [12–15] and physical properties [16–18]. Second, with the increasing Al content, the main phase of the alloy moves from pure face-centered-cubic (FCC) to FCC + pure body-centered-cubic (BCC), and pure BCC phase, making the mechanical and physical properties adjustable [16–25]. Thus, the microstructure, phases and properties of this alloy system have been intensively investigated. In this study, a binary phase

(FCC + BCC) $\text{Al}_{0.5}\text{CoCrFeNi}$ HEA with a balanced strength and plasticity are chosen to investigate the effect of cold rolling on the subsequent solid state phase transformation kinetics.

2. Experimental Procedures

The ingots with a nominal composition of $\text{Al}_{0.5}\text{CoCrFeNi}$ were prepared by melting pure elements (at least 99.95 wt.%) in a vacuum induction-melting furnace. The furnace is firstly heated to 500 °C and held for 2 h to remove the water vapor, and vacuumed to below 10 Pa. Then pure argon is backfilled to expel the rest of air until the vacuum goes back to standard atmospheric pressure. This process is repeated three times in order to gain an oxygen-free environment as much as possible. Afterwards, melting and casting is performed with the protection of high purity argon and the alloy is heated at about 1550 °C for 15 min. Approximately 15 kg ingot is produced by casting the melt into a steel crucible with a height of 180 mm, upper inner diameter of 140 mm and bottom inner diameter of 130 mm.

Samples with the size of $8 \times 20 \times 70 \text{ mm}^3$ are taken from the center of the ingot. Then, the sample is cold rolled to a thickness reduction of 20%. Then, samples were machined to $\phi 6 \times 25 \text{ mm}$ for thermal expansion measurement both from as-cast and cold rolled plates. The thermal expansion curves were tested using a Netzsch® DIL-402C dilatometer (Selb, Germany) under the protection of argon with constant heating rate of 4 K/min, 6 K/min, 8 K/min and 10 K/min.

The microstructure and phases were characterized by scanning electron microscope (SEM, TESCAN MIRA3 XMU (Brno, Czech Republic), and the working distance and the energy of beam used are 15 mm and 20 kV, respectively) and X-ray diffractometer (XRD, DX 2700 (Dandong, China), and the voltage and current used during measurement are 40 kV and 30 mA, respectively), respectively. Uniaxial tensile tests are carried out with a MTS SANS CMT5105 (Shenzhen, China) mechanical tester at the strain rate of 10^{-3} s^{-1} and the specimens are prepared along the rolling direction (RD) direction.

3. Results and Discussion

3.1. Microstructure

The microstructure and XRD patterns of $\text{Al}_{0.5}\text{CoCrFeNi}$ high-entropy alloys at as-cast and 20% cold rolled (CR) condition are shown in Figures 1 and 2. Except for the grain after cold rolling showing a very small amount elongation along the rolling direction, the as-cast and cold rolled sample show quite similar microstructure (Figure 1). Both the samples are mainly FCC phase together with a small amount of BCC phase (Figure 2), indicating 20% cold rolling has no significant effect on the microstructure and phase transition of the $\text{Al}_{0.5}\text{CoCrFeNi}$ high-entropy alloy.

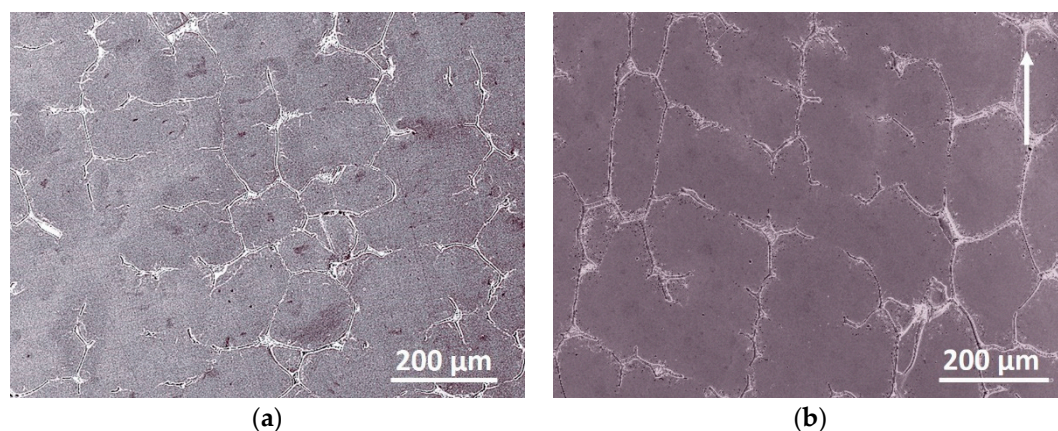


Figure 1. The microstructure of the $\text{Al}_{0.5}\text{CoCrFeNi}$ high-entropy alloys at (a) as-cast and (b) 20% cold rolled condition. The arrow represents the rolling direction.

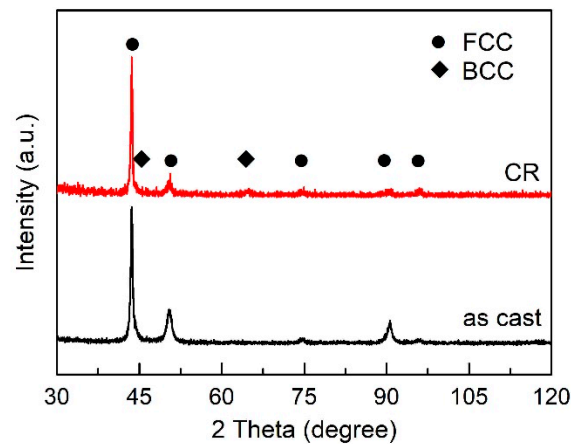


Figure 2. The XRD patterns of $\text{Al}_{0.5}\text{CoCrFeNi}$ high-entropy alloy at as-cast and 20% cold rolled condition.

3.2. Transformed Volume Fraction

Figure 3a shows the thermal expansion curves of $\text{Al}_{0.5}\text{CoCrFeNi}$ HEA at as-cast and 20% CR condition measured at the heating rate of 10 K/min. There is a peak around 1100 K for both curves indicating a phase transition exist, which is proved to be an FCC-BCC phase transition [8]. The first step for phase transition kinetic analysis is to determine the phase transformed volume fraction (f) as a function of temperature or time. Figure 3b shows how to calculate the phase transformed volume as a function of temperature with lever rule method using thermal expansion curves shown in Figure 3a. The lines AD and BE can be obtained by extending the linear expansion section of the thermal expansion curve. Then, the point C is the intersection of AC and thermal expansion curve ($f = 0$ when C is at point D and $f = 100\%$ when C is point E). Finally, the theoretical volume fraction of phase transition can be calculated using the simple lever rule method assuming the volume changes of phase transition is in proportion to the length variations, which is expressed in Equation (1) [26]:

$$f = \frac{|AC|}{|AB|}, \quad (1)$$

where f is the volume fraction, and $|AC|$ and $|AB|$ are the length of the dashed line shown in Figure 3b, indicating the instant thermal expansion length and overall length, respectively.

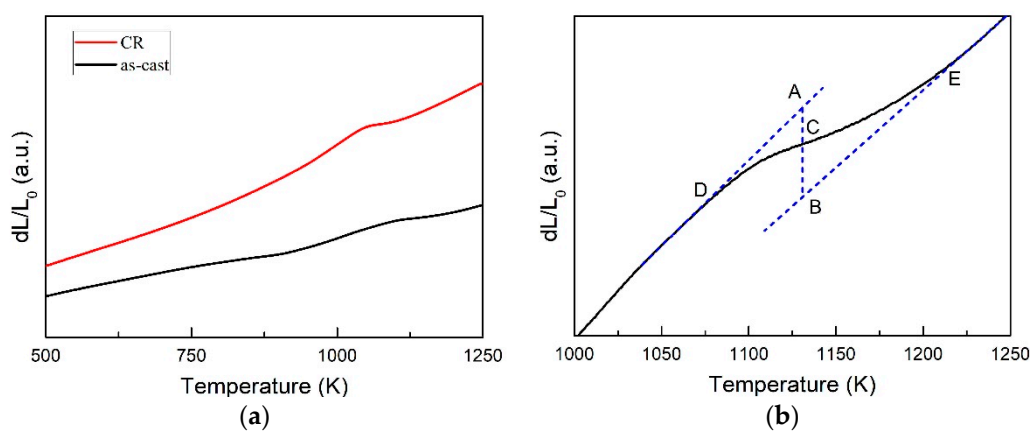


Figure 3. (a) thermal expansion curves of $\text{Al}_{0.5}\text{CoCrFeNi}$ high-entropy alloy measured at as-cast and 20% cold rolled condition at heating rate of 10 K/min; (b) an example of as-cast sample shows how to calculate the phase transformed volume fraction as function of temperature.

Figure 4 shows the transformed volume fraction as a function of temperature at different heating rates for the as-cast (Figure 4a) and 20% CR (Figure 4b) samples. All of the f - T curves show the similar “S” type trend, indicating that the transformation is controlled by a typical nucleation-growth mechanism [27]. Compared with the as-cast sample, it can be seen from Figure 4 that the phase transition of cold rolled sample starts at a much higher temperature (1033 K and 1055 K at 4 K/min for as-cast and cold rolled samples, respectively) but ends at a much lower temperature (1195 K and 1151 K at 4 K/min for as-cast and cold rolled samples, respectively), indicating a much higher transformation rate when the sample is deformed.

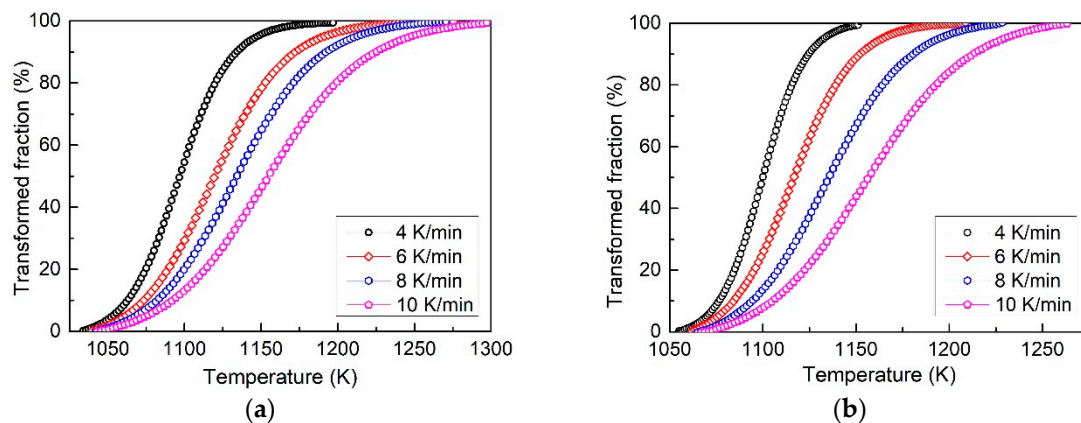


Figure 4. The phase transformed volume fraction as a function of temperature curves of (a) as-cast and (b) 20% cold rolled $\text{Al}_{0.5}\text{CoCrFeNi}$ high-entropy alloy.

3.3. Activation Energy

Activation energy (E) and kinetic exponent (n) are the two most important kinetic parameters. Activation energy is the parameter that can assess phase transition energy barrier. The Kissinger–Akahira–Sunose (KAS) method [28] and Friedman method [29] can be used for the determination of activation energies. Here, we use KAS method, which has the following form [28]:

$$\ln\left(\frac{T^2}{\phi}\right) = -C + \frac{E}{RT}, \quad (2)$$

where T is temperature at certain transformed volume fraction, ϕ is the heating rate, E is the activation energy, C is a constant and R is the molar gas constant. Assuming the activation energy is the same at the same transformed fraction at different heating rates, then, by linear regression between $\ln(T^2/\phi)$ and $1/T$ using the data taken from Figure 4, the activation energy can be directly determined by the slope of the curve.

The determined activation energy E for as cast and 20% CR $\text{Al}_{0.5}\text{CoCrFeNi}$ HEA at four different transformed volume fractions, $f = 0.2, 0.4, 0.6$ and 0.8 are shown in Figure 5. The activation energies of as-cast and 20% CR $\text{Al}_{0.5}\text{CoCrFeNi}$ HEA show the same decreasing trend with the increasing transformed volume fraction, f , however, the value are quite different. For the as-cast sample, the activation energies are 262 kJ/mol and 126 kJ/mol when transformed volume fraction is 0.2 and 0.8, respectively. The mean value is 181 kJ/mol—while, for the 20% CR sample, E are 223 kJ/mol and 110 kJ/mol when transformed volume fraction is 0.2 and 0.8, respectively. The average activation energy is 159 kJ/mol, which is 10% lower than the as-cast sample, indicating that the phase transformation process of the deformed sample is much easier than the as-cast sample.

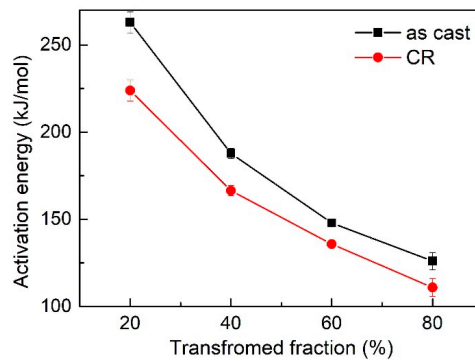


Figure 5. The activation energies at different phase transformed volume fractions for as-cast and cold rolled $\text{Al}_{0.5}\text{CoCrFeNi}$ high-entropy alloys calculated using the KAS method.

3.4. Kinetic Exponent

The kinetic exponent, also called the Avrami exponent, is a key kinetic parameter that can directly obtain the phase transition mode. The kinetic exponent is generally determined based on the well-known Johnson–Mehl–Avrami (JMA) model [30], which has the following form:

$$f = 1 - \exp(-Kt^n), \quad (3)$$

where n is the Avrami exponent, K is a rate constant and t is the time. In case of phase transformations that are carried out at constant heating rate, the time can be expressed as [31]:

$$t - t_0 = \frac{T - T_0}{\varnothing}, \quad (4)$$

where T_0 and t are the starting temperature and time of phase transition. Then, the kinetic exponent can be obtained by some mathematical treatment of Equations (3) and (4), which can be expressed as:

$$n = - \frac{\ln(-\ln(1-f))}{\frac{E}{RT}}. \quad (5)$$

Based on Equation (5), we can determine the kinetic exponent n from the slope of $\ln(-\ln(1-f))$ vs. $1/T$ curve.

For a real phase transformation, n will change with the transformed volume fraction. A simple derivative equation of Equation (5) can determine the Avrami exponent as variables, which has been used in many previous published papers [31–33]. In this case, n is called local Avrami exponent, which can be described as:

$$n = - \frac{\partial \ln(-\ln(1-f))}{\partial \frac{E}{RT}}. \quad (6)$$

By taken the activation energy at a different transformed volume fraction using Equation (2), Avrami exponent n can be calculated by the differential of the curve of $E/RT - \ln[-\ln(1-f)]$. Figure 6 represents the kinetic exponent at different transformed volume fractions at the heating rate 10 K/min for the as-cast and deformed samples. According to Figure 6, two important pieces of information can be drawn. First, both of the as-cast and deformed samples show three typical stages of transformation: (I) rapid decrease of the kinetic exponent when $f < 5\%$, indicating that the nucleation rate of the sample is decreasing at the beginning; (II) slow decrease of the kinetic exponent from 4 to 1.5 during $9\% < f < 95\%$, indicating the decreasing nucleation rate, and the growth mode of the nuclei changes from interface controlled to diffusion controlled; (III) strong increase of the kinetic exponent when $f > 95\%$, an indication that some new inhomogeneous nucleation occurs inside the sample. Second the kinetic exponent, n , is higher for the sample pre-deformed than the as-cast sample. This means that the

nucleation rate of the deformed sample is much higher and the growth of the nuclei is much easier than the as-cast sample.

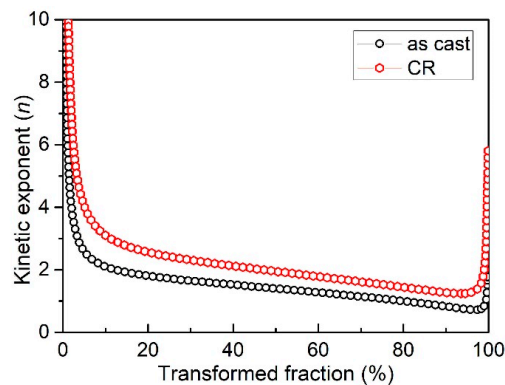


Figure 6. Variation of n with phase transformed fraction for as-cast and deformed $\text{Al}_{0.5}\text{CoCrFeNi}$ high-entropy alloy at the heating rate of 10 K/min.

3.5. Discussion

For the deformed sample like cold rolling, normally, there will be an anisotropic effect due to the stress state during deformation are different at different directions. For the cold rolled sample, the rolling direction (RD) and the transverse direction (TD) always owns different textures, stress and properties. For the above results, all of the analysis is based on the sample that is taken from the RD direction. Figure 7 shows the thermal expansion curves that are both taken from the RD and TD direction of a 20% CR sample. According to the figure, it can be seen that the rolling direction has quite a limited effect on the thermal expansion behavior. The reason may be due to the fact that a 20% reduction is not large enough to generate a big difference, and it can also be found from Figure 1 that the CR sample has a similar microstructure as the as-cast sample. Large differences can be made evident at much larger CR reduction thickness, and the grain will be severely deformed and elongated along the rolling direction [12]. In this case, the thermal expansion behavior could be different for different directions. Thus, it can be concluded that there is no typical anisotropic effect in the 20% CR sample, and, during the solid state phase transformation process, the nucleation and growth process can be treated as homogeneous.

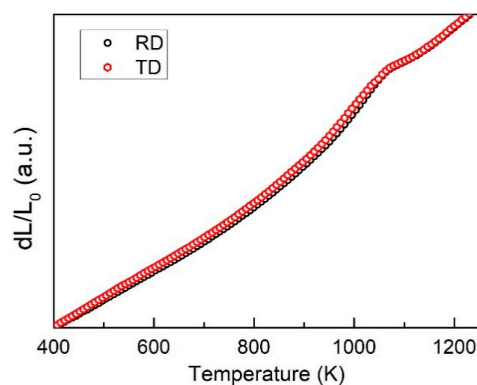


Figure 7. The thermal expansion curves of the samples taken from the rolling direction (RD) and transverse direction (TD) for 20% cold rolled $\text{Al}_{0.5}\text{CoCrFeNi}$ high-entropy alloy measured at the heating rate of 10 K/min.

There is not much difference for the microstructure (Figure 1) and phases (Figure 2) between the as-cast and deformed sample; however, according to the f - T curve, activation energy and kinetic exponent, there is a large difference. The microstructure of $\text{Al}_x\text{CoCrFeNi}$ ($0 \leq x \leq 2$) HEAs has

been intensively investigated in different heat treatment conditions [17–25]. Different from the thermo-mechanical processing that can affect the transformation pathways in $\text{Al}_{0.3}\text{CoCrFeNi}$ [34], 20% cold rolling cannot alter the phase transition product [12]. Thus, the microstructure and phases exhibit no difference as shown in Figures 1 and 2. However, the deformed sample shows a much faster transformation rate, much lower activation energy and much larger kinetic exponents, an indication of a large difference for the transformation kinetics. Figure 8 exhibits the tensile stress–strain curves of $\text{Al}_{0.5}\text{CoCrFeNi}$ HEAs at as-cast and 20% CR conditions. There exists a large difference: the deformed sample shows a much larger stress but lower plasticity. The yield stress increased from 402 MPa (as-cast sample) to 755 MPa (CR sample), while the strain decreased from 33.7% (as-cast sample) to 6.2% (CR sample), indicating a strong strain-hardening effect of the cold rolling. In the present study, due to the small reduction rate of the CR, there is not much difference in the macroscopic microstructure; however, 20% CR is enough to generate a large crystal lattice distortion, and many crystal defects, like vacancy, dislocation and substructure inside the grain. Then, the deformed sample stored a large quantity of energy, which is beneficial for the phase transition during the continuous heating. Thus, because of all the above factors that are generated by cold rolling, the deformed sample shows a much higher transformation rate since all the defects and stored energy inside the sample can promote the nucleation rate and grain growth speed.

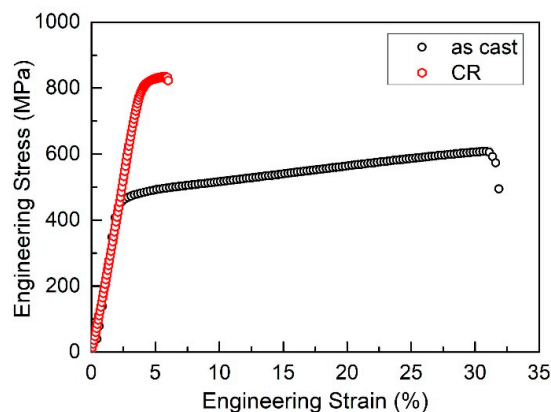


Figure 8. The engineering stress–strain curves of $\text{Al}_{0.5}\text{CoCrFeNi}$ high-entropy alloys at as-cast and 20% CR conditions.

4. Conclusions

The effects of cold rolling on the phase transformation kinetics of an $\text{Al}_{0.5}\text{CoCrFeNi}$ high-entropy alloy are studied by the thermal expansion method. The transformed volume fraction–temperature curves of as-cast and 20% cold rolling $\text{Al}_{0.5}\text{CoCrFeNi}$ high-entropy alloys are determined by the lever rule method using thermal expansion curves. Using the KAS method, the mean activation energy for as-cast and deformed HEAs calculated are 181 kJ/mol and 159 kJ/mol, respectively. The kinetic exponent is determined using the local Avrami exponent method based on the JMA equation. Both as-cast and deformed samples show the three stages of kinetic exponent variations, and the deformed alloy shows a much larger value compared with the as-cast alloy, indicating a much higher nucleation and growth rate. The reason for the kinetic exponent variations are thought to be related with the deformation induced strain and defects inside the sample that can generate a much higher energy that favors the nucleation and growth process.

Author Contributions: Conceptualization, J.W. and J.S.L.; Investigation, J.W., H.X.Y., T.G., J.X.W.; Writing—original draft, J.W., H.X.Y., T.G.; Writing—review & editing, J.W., W.Y.W., J.S.L.

Funding: This research was funded by the Natural Science Foundation of China, grant number 51571161 and 51774240 and the fund of State Key Laboratory of Solidification Processing in NWPU, grant number 121-TZ-2015.

Conflicts of Interest: The authors declare no conflict of interest.

References

1. Cantor, B.; Chang, I.T.H.; Knight, P.; Vincent, A.J.B. Microstructural development in equiatomic multicomponent alloys. *Mater. Sci. Eng. A* **2004**, *375–377*, 213–218. [[CrossRef](#)]
2. Yeh, J.W.; Chen, S.K.; Lin, S.J.; Gan, J.Y.; Chin, T.S.; Shun, T.T.; Tsau, C.H.; Chang, S.Y. Nanostructured high-entropy alloys with multiple principal elements: Novel alloy design concepts and outcomes. *Adv. Eng. Mater.* **2004**, *6*, 299–303. [[CrossRef](#)]
3. Zhang, W.; Liaw, P.K.; Zhang, Y. Science and technology in high-entropy alloys. *Sci. China Mater.* **2018**, *61*, 2–22. [[CrossRef](#)]
4. Miracle, D.B.; Senkov, O.N. A critical review of high entropy alloys and related concepts. *Acta Mater.* **2017**, *122*, 448–511. [[CrossRef](#)]
5. Wang, J.; Li, J.; Wang, J.; Bu, F.; Kou, H.; Li, C.; Zhang, P.; Beaugnon, E. Effect of Solidification on Microstructure and Properties of FeCoNi(AlSi)_{0.2} High-Entropy Alloy Under Strong Static Magnetic Field. *Entropy* **2018**, *20*, 275. [[CrossRef](#)]
6. Tsai, M.H. Physical Properties of High Entropy Alloys. *Entropy* **2013**, *15*, 5338–5345. [[CrossRef](#)]
7. Klimova, M.; Stepanov, N.; Shaysultanov, D.; Chernichenko, R.; Yurchenko, N.; Sanin, V.; Zherebtsov, S. Microstructure and Mechanical Properties Evolution of the Al, C-Containing CoCrFeNiMn-Type High-Entropy Alloy during Cold Rolling. *Materials* **2018**, *11*, 53. [[CrossRef](#)] [[PubMed](#)]
8. Wang, J.; Niu, S.; Guo, T.; Kou, H.; Li, J. The FCC to BCC phase transformation kinetics in an Al_{0.5}CoCrFeNi high entropy alloy. *J. Alloy. Compd.* **2017**, *710*, 144–150. [[CrossRef](#)]
9. Liu, F.; Sommer, F.; Bos, C.; Mittemeijer, E.J. Analysis of solid state phase transformation kinetics: Models and recipes. *Inter. Mater. Rev.* **2007**, *52*, 193–212. [[CrossRef](#)]
10. Zhang, Y.; Li, J.; Wang, J.; Niu, S.; Kou, H. Hot deformation behavior of as-cast and Homogenized Al_{0.5}CoCrFeNi High Entropy Alloys. *Metals* **2016**, *6*, 277. [[CrossRef](#)]
11. Li, D.; Zhang, Y. The ultrahigh charpy impact toughness of forged Al_xCoCrFeNi high entropy alloys at room and cryogenic temperatures. *Intermetallics* **2016**, *70*, 24–28. [[CrossRef](#)]
12. Guo, T.; Li, J.; Wang, J.; Wang, W.Y.; Liu, Y.; Luo, X.; Kou, H.; Beaugnon, E. Microstructure and properties of bulk Al_{0.5}CoCrFeNi high-entropy alloy by cold rolling and subsequent annealing. *Mater. Sci. Eng. A* **2018**, *729*, 141–148. [[CrossRef](#)]
13. Zhang, Y.; Li, J.; Wang, J.; Wang, W.Y.; Kou, H.; Beaugnon, E. Temperature dependent deformation mechanisms of Al_{0.3}CoCrFeNi high-entropy alloy, starting from serrated flow behavior. *J. Alloy. Compd.* **2018**, *757*, 39–43. [[CrossRef](#)]
14. Niu, S.; Kou, H.; Guo, T.; Zhang, Y.; Wang, J.; Li, J. Strengthening of nanoprecipitations in an annealed Al_{0.5}CoCrFeNi high entropy alloy. *Mater. Sci. Eng. A* **2016**, *671*, 82–86. [[CrossRef](#)]
15. Li, D.; Li, C.; Feng, T.; Zhang, Y.; Sha, G.; Lewandowski, J.J.; Liaw, P.K.; Zhang, Y. High-entropy Al_{0.3}CoCrFeNi alloy fibers with high tensile strength and ductility at ambient and cryogenic temperatures. *Acta Mater.* **2017**, *123*, 285–294. [[CrossRef](#)]
16. Yang, T.; Xia, S.; Liu, S.; Wang, C.; Liu, S.; Fang, Y.; Zhang, Y.; Xue, J.; Yan, S.; Wang, Y. Precipitation behavior of Al_xCoCrFeNi high entropy alloys under ion irradiation. *Sci. Rep.* **2016**, *6*, 32146. [[CrossRef](#)] [[PubMed](#)]
17. Chou, H.P.; Chang, Y.S.; Chen, S.K.; Yeh, J.W. Microstructure, thermophysical and electrical properties in Al_xCoCrFeNi (0 ≤ x ≤ 2) high-entropy alloys. *Mater. Sci. Eng. B* **2009**, *163*, 184–189. [[CrossRef](#)]
18. Kao, Y.F.; Chen, S.K.; Chen, T.J.; Chu, P.C.; Yeh, J.W.; Lin, S.J. Electrical, magnetic, and Hall properties of Al_xCoCrFeNi high-entropy alloys. *J. Alloy. Compd.* **2011**, *509*, 1607–1614. [[CrossRef](#)]
19. Kao, Y.F.; Lee, T.D.; Chen, S.K.; Chang, Y.S. Electrochemical passive properties of Al_xCoCrFeNi (x = 0, 0.25, 0.50, 1.00) alloys in sulfuric acids. *Corros. Sci.* **2010**, *52*, 1026–1034. [[CrossRef](#)]
20. Jasiewicz, K.; Cieslak, J.; Kaprzyk, S.; Tobola, J. Relative crystal stability of Al_xFeNiCrCo high entropy alloys from XRD analysis and formation energy calculation. *J. Alloy. Compd.* **2015**, *648*, 307–312. [[CrossRef](#)]
21. Xia, S.Q.; Yang, X.; Yang, T.F.; Liu, S.; Zhang, Y. Irradiation Resistance in Al_xCoCrFeNi High Entropy Alloys. *JOM* **2015**, *67*, 2340–2344. [[CrossRef](#)]
22. Nahmany, M.; Hooper, Z.; Stern, A.; Geanta, V.; Voiculescu, I. Al_xCrFeCoNi high-entropy alloys: Surface modification by electron beam bead-on-plate melting. *Metallogr. Microsc. Anal.* **2016**, *5*, 1–12.
23. Zhang, C.; Zhang, F.; Diao, H.; Gao, M.C.; Tang, Z.; Poplawsky, J.D.; Liaw, P.K. Understanding phase stability of Al-Co-Cr-Fe-Ni high entropy alloys. *Mater. Des.* **2016**, *109*, 425–433. [[CrossRef](#)]

24. Ma, Y.; Jiang, B.; Li, C.; Wang, Q.; Dong, C.; Liaw, P.K.; Xu, F.; Sun, L. The BCC/B2 morphologies in $Al_xNiCoFeCr$ high-entropy alloys. *Metals* **2017**, *7*, 57. [CrossRef]
25. Rao, J.C.; Diao, H.Y.; Ocelík, V.; Vainchtein, D.; Zhang, C.; Kuo, C.; Tang, Z.; Guo, W.; Poplawsky, J.D.; Zhou, Y.; et al. Secondary phases in $Al_xCoCrFeNi$ high-entropy alloys: An in-situ TEM heating study and thermodynamic appraisal. *Acta Mater.* **2017**, *131*, 206–220. [CrossRef]
26. Kou, H.C.; Wang, J.; Chang, H.; Tang, B.; Li, J.S.; Hu, R.; Zhou, L. Kinetic analysis of the isochronal crystallization of $Ti_{40}Zr_{25}Ni_8Cu_9Be_{18}$ metallic glass. *J. Non-Cryst. Solids* **2009**, *355*, 420–424. [CrossRef]
27. Christian, J.W. *Theory of Transformations in Metals and Alloys*, 3rd ed.; Pergamon Press: Oxford, UK, 2002.
28. Kissinger, H.E. Reaction Kinetics in Differential Thermal Analysis. *Anal. Chem.* **1957**, *29*, 1702–1706. [CrossRef]
29. Bertolino, V.; Cavallaro, G.; Lazzara, G. Effect of the biopolymer charge and the nanoclay morphology on nanocomposite materials. *Ind. Eng. Chem. Res.* **2016**, *55*, 7373–7380. [CrossRef]
30. Wang, J.; Kou, H.C.; Li, J.S.; Gu, X.F.; Zhong, H.; Chang, H.; Zhou, L. An integral fitting method for analyzing the isochronal transformation kinetics: Application to the crystallization of a Ti-based amorphous alloy. *J. Phys. Chem. Solids* **2009**, *70*, 1448–1453. [CrossRef]
31. Majhi, K.; Varma, K.B.R. Crystallization kinetic studies of $CaBi_2B_2O_7$ glasses by non-isothermal methods. *J. Mater. Sci.* **2009**, *44*, 385–391. [CrossRef]
32. Lu, W.; Niu, J.; Wang, T.; Xia, K.; Xiang, Z.; Song, Y.; Mi, Z.; Zhang, W.; Tian, W.; Yan, Y. Phase transformation kinetics and microstructural evolution of MnAl permanent magnet alloys. *J. Alloy. Compd.* **2016**, *685*, 992–996. [CrossRef]
33. Zhou, Z.; Lai, M.; Tang, B.; Kou, H.; Chang, H.; Zhu, Z.; Li, J.; Zhou, L. Non-isothermal phase transformation kinetics of ω phase in TB-13 titanium alloys. *Mater. Sci. Eng. A* **2010**, *527*, 5100–5104. [CrossRef]
34. Gwalani, B.; Gorsse, S.; Choudhuri, D.; Styles, M.; Zheng, Y.; Mishra, R.S.; Banerjee, R. Modifying transformation pathways in high entropy alloys or complex concentrated alloys via thermo-mechanical processing. *Acta Mater.* **2018**, *153*, 169–185. [CrossRef]



© 2018 by the authors. Licensee MDPI, Basel, Switzerland. This article is an open access article distributed under the terms and conditions of the Creative Commons Attribution (CC BY) license (<http://creativecommons.org/licenses/by/4.0/>).